Polymer Journal

REGULAR ARTICLE

Thermal Degradation Behavior of Polystyrene/Magadiite Nanocomposites Prepared by Surface-initiated Nitroxide-Mediated Radical Polymerization

By Hideaki YUKUTAKE,[1,] Motoyasu KOBAYASHI,[2] Hideyuki OTSUKA,[2] and Atsushi TAKAHARA[2]*

Exfoliated polystyrene (PS)/magadiite nanocomposites with a high suppression effect on thermal degradation were successfully prepared by *in situ* nitroxide-mediated radical polymerization of styrene monomer from the magadiite interlayer surface. Surface-initiated polymerization of styrene was conducted from the radical initiators immobilized on magadiite at 398 K. The number-average molecular weight (M_n) of the grafting PS increased with monomer conversion keeping a relatively low polydispersity index. The initiator efficiency was estimated to be less than 10% by size exclusion chromatography analysis. The results of X-ray diffraction and transmission electron microscopy suggested that the nanocomposites provided exfoliated structures. The fine dispersion state of magadiite in PS matrices contributed to effective suppression of the thermal degradation of PS. In addition, an interesting difference in the shape of the final residues was observed. Thermal decomposition of exfoliated PS/magadiite nanocomposites gave a substantial rigid solid as a residue, the shape of which largely depended on the concentrations of magadiite in the PS matrices. For instance, the thermal decomposition of nanocomposites produced a seamless residue that can effectively retard the decomposition rate. In contrast, the simple mixture of PS and magadiite was thermally decomposed to be powdery ash in the final residues.

KEY WORDS: Nanocomposites / Magadiite / Surface-Initiated Polymerization / Exfoliated Structures / Polystyrene / Flame-Retardant Compounds / Thermal Degradation /

Various types of flame-retardant compounds have been blended into polymers to improve their incombustibilities. Traditional flame-retardant compounds include halogenated, phosphorous, and inorganic compounds. However, polymer composites containing halogenated compounds generate toxic and corrosive gases during their combustion. The use of some halogenated flame-retardant compounds has been restricted by international regulation due to the potential for environmental damage and threats to human health.[1] Some phosphorous flame retardants might also present a risk to the environment. Both magnesium hydroxide and aluminum hydroxide show originally poor incombustibility, but large quantities of inorganic components should be introduced into polymer matrices in order to attain sufficient incombustibility, leading to the deterioration of physical properties in polymer materials.

Therefore, a new concept of alternative flame-retardant compounds has been expected. With the advancement of nanotechnology, research regarding hybrid polymeric materials containing nanoparticle fillers has attracted much attention because some nanoparticle fillers dispersed in the polymer matrices can improve mechanical[2–4] and incombustible[5–13] properties. In addition, they are environmentally benign compared with conventional flame-retardant compounds. Nanoparticle fillers for flame-retardant compounds include clays,[5,6] nanoparticles,[7,8] carbon nanotubes (CNT),[9–11] and polyhedral silsesquioxanes.[12,13] Of these, clays are one of the most practical materials with respect to cost. However, clays have multilayer structures in which the individual layers are strongly stacked together by electrostatic interactions; it is therefore difficult to disperse the clays at the nano scale into non-polar polymeric materials such as polypropylene and polystyrene (PS). An initiator for nitroxide-mediated polymerization has recently been immobilized onto a montmorillonite (MMT) or hectorite (HT) interlayer surface using electrostatic interactions to successfully prepare exfoliated PS/clay nanocomposites by means of *in situ* living free radical polymerization of styrene from each interlayer surface.[14,15] Their dispersion in the PS matrices is probably better than that in any conventional PS/clay nanocomposites.

The flame retardancy of composites is strongly dependent on the dispersion state of the fillers. It has been reported that the flame retardancy improves with better dispersion, higher loading, and a higher interface area (aspect ratio) of the nanotubes.[11,16] This tendency can be expected to be observed in polymer/clay systems; in other words, clays with better dispersion and higher aspect ratio should exhibit higher flame retardancy.

In the present study, we focused on "magadiite," which belongs to the family of layered sodium silicates with a relatively high aspect ratio.[17,18] An effective reduction in the combustibility of PS/magadiite composites has thus far not been observed due to the difficulty of dispersing magadiite in non-polar polymers such as PS matrix.[19] In contrast to MMT and HT, magadiite does not consist of alumina silicates but

[1]ADEKA Corporation, 5-2-13 Shirahata, Minami-ku, Saitama 336-0022, Japan
[2]Institute for Materials Chemistry and Engineering, Kyushu University, 744 Motooka, Nishi-ku, Fukuoka 819-0395, Japan
*To whom correspondence should be addressed (Tel: +81-48-838-2222, Fax: +81-48-838-2250, E-mail: yukutake@adeka.co.jp).

instead silicates alone, and reactive hydroxyl groups present on the interlayer surface.[20] The hydroxyl groups can form covalent bonds with specific organosilanes to immobilize them onto the interlayer surface. In contrast, clays such as MMT, HT, and, mica, which are 2:1 type clay minerals, do not have reactive hydroxyl groups on the interlayer surface; therefore, the approach to introducing organic compounds onto the interlayer surface is limited to the utilization of electrostatic force between alkylammonium salts and clay platelets. For this case, the low thermal stability of ammonium salts could result in thermal degradation at high temperatures during extrusion and molding processes, causing problems such as offensive amine smells and coloration.[21]

In the present study, we attempted to immobilize the magadiite interlayer surface with the initiator through the formation of covalent bonds, and to obtain exfoliated PS/magadiite nanocomposites by means of surface-initiated polymerization of styrene monomer from the interlayer surface. Additionally, the relationship between various dispersion states of magadiite in a series of PS/magadiite composites and their thermal degradation behaviors was examined.

EXPERIMENTAL

Materials

Styrene was purchased from Kanto Chemical Co., Inc. and purified by distillation under reduced pressure over calcium hydride. 4-Methoxy-2,2,6,6-tetramethylpiperidine-1-oxyl was provided from ADEKA Co., Ltd. and a hydroxy functionalized alkoxyamine **2** shown in Scheme 1 was synthesized with reference to the literature.[22] Cyclopentadienyl platinum (II) dichloride (Cp_2PtCl_2) used as a catalyst for hydrosilylation was prepared according to the literature.[23] Magadiite was prepared by means of hydrothermal synthesis according to the literature.[24,25] The average size of magadiite platelets was estimated to be approximately 0.8 μm by scanning transmission electronic microscopy observation. Dodecyltrimethylammonium chloride (DTMA) was purchased from Tokyo Chemical Industry Co., Ltd. Magadiite modified with DTMA (DTMA-magadiite) was prepared with reference to the literature.[17]

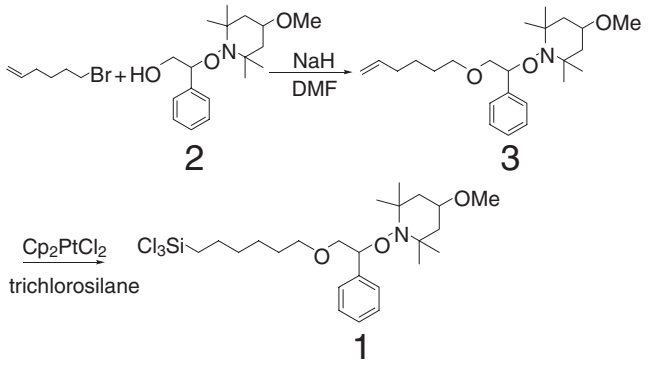

Scheme 1. Synthetic route for a nitroxide-mediated radical initiator with trichlorosilane.

Magadiite immobilized with trimethylsilane (TMS-magadiite) was provided from ADEKA Co., Ltd. and used as received. Pure polystyrene (pure PS) (M_w: 200k) was purchased from Scientific Polymer Products, Inc. Other commercial reagents were purchased from Sigma-Aldrich Japan K.K., Tokyo Chemical Industry Co., Ltd., Kanto Chemical Co., Inc., and Kokusan Chemical Co., Ltd. They were used without further purification. Analytical thin-layer chromatography (TLC) was performed on commercial Merck plates coated with silica gel $60\,F_{254}$ (20×20 cm). Wakogel C-200 (particle size 75–150 μm), which was used as silica gel for chromatography and as a starting material for magadiite, was purchased from Wako Pure Chemical Industries, Ltd. Omnipore membrane filter (0.1 μm) was purchased from Millipore Corporation.

Preparation of Nitroxide-Mediated Radical Initiator with Trichlorosilane and Various PS/Magadiite Nanocomposites

1-(3′-Oxa-1′-phenyl-8′-noneneoxy)-4-methoxy-2,2,6,6-tetramethylpiperidine, 3. Scheme 1 exhibits the reaction scheme of a nitroxide-mediated radical initiator **1** with a trichlorosilane group. To a solution of hydroxy functionalized alkoxyamine **2** (114 mmol) in 150 mL of dimethylformamide (DMF), sodium hydride (126 mmol) was added with ice-bath cooling, and the reaction mixture was then stirred at room temperature under N_2 for 30 min. A solution of 6-bromohexene (125 mmol) in 20 mL of DMF was added dropwise to the reaction mixture that was stirred at room temperature for 24 h. The completion of the reaction was confirmed by TLC. To the reaction mixture was added 100 mL of distilled water and 200 mL of *n*-hexane, and the organic layer was recovered. The aqueous layer was then extracted twice with 200 mL of *n*-hexane. The combined organic extracts were dried over anhydrous magnesium sulfate and concentration by evaporation. The crude product was purified by flash column chromatography with *n*-hexane to give **3** (29.6 g, 66.7%). FT-IR (neat) the stretching vibration absorption of aromatic CH and aliphatic double bond CH around 3100–3062 cm^{-1}, the stretching vibration absorption of aliphatic CH_3, CH_2, and CH around 2940–2850 cm^{-1}. The overtone bands of mono-substituted benzene ring around 2000–1700 cm^{-1}; ^1H NMR ($CDCl_3$) δ (ppm) 0.90–1.75 (m, 20H), 1.85–2.00 (q, 2H), 3.48–3.88 (dd, 2H), 4.72–4.75 (t, 1H) 4.82–4.94 (t, 2H) 5.62–5.74 (m, 1H), 7.14–7.30 (m, 5H, aromatic); ^{13}C NMR ($CDCl_3$) 21.30, 25.29, 29.00, 29.69, 33.43, 55.69, 71.06, 71.70, 73.44, 85.58, 114.27, 127.29, 127.78, 127.82, 138.80.

1-(3′-Oxa-1′-phenyl-9′-trichlorosilylnonyloxy)-4-methoxy-2,2,6,6-tetramethylpiperidine, 1. To alkene **3** (0.457 mmol) and 10 mg of Cp_2PtCl_2 in 1 mL of chloroform was added trichlorosilane (29.7 mmol), and the reaction mixture was stirred at 303 K under N_2 for 5 h. The completion of the reaction was confirmed by ^1H NMR. The excessive amounts of trichlorosilane were removed by reduced pressure to give **1**. The crude product (1.56 g) was used for the next reaction without further purification. ^1H NMR ($CDCl_3$) δ (ppm) 1.05–2.70 (m, 26H), 3.20–3.95 (m, 8H), 6.00–6.20 (m, 1H), 7.23–7.36 (m, 3H, aromatic), 7.41–7.50 (m, 2H, aromatic).

Immobilization of Initiator 1 onto the Magadiite Interlayer Surface (1-magadiite). 0.5 g of DTMA-magadiite was introduced into a 4-necked flask and solution was stirred at 393 K under reduced pressure for 2 h, then cooled to room temperature under ambient pressure. Initiator **1** (6.5 mmol) dissolved in 50 mL of chloroform was added to the dried DTMA-magadiite, and the mixture was stirred at room temperature under N_2 for approximately 100 h. The solid mass was dispersed in each solution, including *n*-hexane, acetone, and distilled water, by ultra sonication for 3 min and centrifuged twice. Chlorine present in the solid mass was eliminated by an alkali washing. Furthermore, the solid mass was washed with distilled water and acetone and then collected with a 0.1 μm membrane filter. The solid mass was dried *in vacuo* at room temperature for 12 h to give 0.44 g of **1**-magadiite.

Preparation of Exfoliated PS/Magadiite Nanocomposites Films. Into a glass tube were introduced **1**-magadiite and styrene, which were then degassed by ten freeze-pump-thaw cycles under Ar atmosphere. Polymerization was carried out at 398 K for various times of 1, 3, and 6 h in the closed system. The reaction was quenched by cooling and the addition of a small amount of acetone. The solid was dispersed in acetone solution by ultra sonication and then collected repeatedly by centrifugation in order to remove unbounded PS from the magadiite surface. The solid was recovered with a 0.1 μm membrane filter and then dried *in vacuo* at room temperature for 24 h to obtain PS/magadiite nanocomposites. The powder of the PS/magadiite nanocomposites was pressed on a hot plate at 573 K to form their films.

Preparation of Various PS/Magadiite Composites by Coagulation Methods.[11] The mixture of 570 mg of pure PS (M_w: 200k) and 30 mg of Na-magadiite was dispersed in 40 mL of toluene by ultra sonication at room temperature for 1 h. The mixture was added dropwise to an excess amount of methanol to precipitate the composites. The residue was dried *in vacuo* at 393 K for 12 h to give PS/Na-magadiite composites. The resultant powder was pressed on a hot stage at 503 K to form their films. PS/TMS-magadiite composites and PS/DTMA-magadiite composites were also prepared through the coagulation method.

Characterization

The number-average weight (M_n) and polydispersity index (PDI) of anchored polymers were determined by size exclusion chromatography (SEC) on a JASCO instrument equipped with a JASCO 830-RI refractive index detector using THF as an eluent, which ran through PS/divinyl benzene gel (PLgel 5 μm MIXED-C column × 3, flow rate 0.8 mL/min) at 313 K. X-Ray powder diffraction (XRD) was performed on an Ultima IV diffractometer (Rigaku Corporation) using $\lambda = 0.15418$ nm at 40 kV of voltage and 40 mA current. The samples were ultramicrotomed with a diamond knife on an EM UC6 Ultramicrotome (Leica Microsystems) at room temperature to create sections 50 nm thick. The sections were transferred from the knife-edge to an elastic carbon support membrane, STEM100Cu grid (Okenshoji Co., Ltd.). Transmission electron microscopy (TEM) images of a series of composites were observed with an H-7500 (Hitachi High-Technologies Corporation) at 100 kV of acceleration voltage, 10 μA of beam current. Optical microscopy images of a series of composites were observed with an Olympus BX-51 (Olympus Corporation) with a hot stage, an LK-600PM (Linkam Scientific Instruments Ltd.), in a nitrogen stream of 50 mL/min at 553 K. Thermogravimetric analysis (TGA) was carried out on a Thermoplus2 TG8120 (Rigaku Corpotration) in a nitrogen stream of 200 mL/min at a scan rate of 10 K/min, ranging from 303 to 1173 K. Scanning transmission electron microscopy (STEM) images of a series of composites after TGA were observed with an S-4800 (Hitachi High-Technologies Corporation) at 20 kV of acceleration voltage and 10 μA of current. ^1H and ^{13}C nuclear magnetic resonance spectra (NMR) were recorded on a JNM-ECX400 (JOEL Ltd.). Fourier-transform infrared spectra (FT-IR) were measured with KBr and neat methods on an FT-IR 8300 (Shimadzu Corporation). The composition of a series of compounds was determined by CHN elemental analysis. X-Ray photoelectron spectroscopy (XPS) was conducted on an AXIS-ULTRA DLD (Kratos Analytical Ltd.).

RESULTS AND DISCUSSION

Characterization of 1-Magadiite

Table I shows the chemical compositions of DTMA-magadiite, **1**-magadiite, and each organic content in the interlayer determined by elemental analysis. Chlorine atoms were not detected in **1**-magadiite by XPS due to the elimination of chlorine during an alkali washing. The observed C/N ratios in both DTMA-magadiite and **1**-magadiite were almost consistent with the corresponding calculated values. The consistency of the C/N ratios shows immobilization of DTMA into initiator **1** on the interlayer surface during the silylated reaction. The organic content present in the interlayer per unit gram of the modified magadiite was calculated to be approximately 1.1 and 0.5 mmol/g, respectively.

The basal spacings of Na-magadiite, **1**-magadiite, and DTMA-magadiite were determined by the XRD patterns shown in Figure 1 to be 1.55, 2.34, and 2.74 nm, respectively. These values correspond almost exactly to the molecular size of the intercalators, indicating that the DTMA form an

Table I. Chemical compositions of DTMA-magadiite, **1**-magadiite, and each organic content in the interlayer

Magadiite derivative	(obs.)				(calc.)
	C (%)	N (%)	C/N[c]	Organic content (mmol/g)	C/N[c]
DTMA-magadiite	20.6	1.57	13.1	1.1[a]	12.9
1-magadiite	14.8	0.7	21.2	0.5[b]	20.6

[a]Organic content = C(%)/[12 × (number of carbon atom in DTMA)] × 1000. [b]Organic content = C(%)/[12 × (number of carbon atom in initiator **1**)] × 1000. [c]Weight ratio.

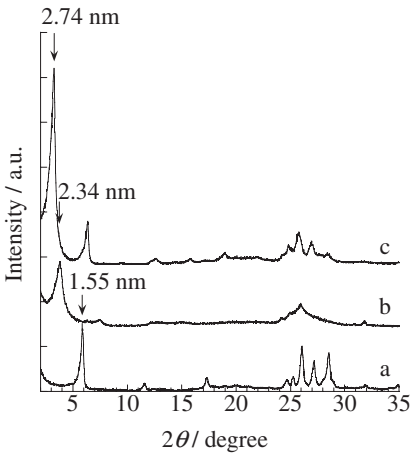

Figure 1. XRD patterns of a series of magadiite derivatives. (a) Na-magadiite; $d_{001} = 1.55$ nm, (b) **1**-magadiite; $d_{001} = 2.34$ nm, and (c) DTMA-magadiite; $d_{001} = 2.74$ nm.

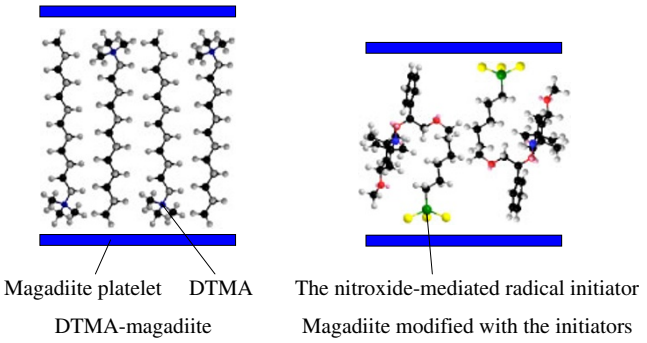

Figure 2. Schematic representation of the speculated conformation of intercalators present in the magadiite interlayer.

extended structure with a *trans* zig-zag conformation,[26] and **1**-magadiite is packed with a folded structure, as shown in Figure 2. The basal spacing of inorganic magadiite (H-magadiite) is approximately 1.12 nm.[27] The long axis distance of DTMA with a *trans* zig-zag conformation and that of folded structures of initiator **1** are estimated to be approximately 1.60 and 1.45 nm by molecular modeling, respectively. The basal spacings are calculated from the sum of the basal spacing of H-magadiite, and the size of each intercalator was determined to be 2.72 and 2.57 nm, respectively, which is slightly different from the observed values. Each small difference in the observed and calculated values on the basal spacings is presumably due to some degree of tilting of the long axis dimensions of intercalators and the presence of H_2O in the interlayer.[28]

Infrared spectra of Na-magadiite and DTMA-magadiite in Figure 3 exhibited absorbance around 3650 cm^{-1} due to the hydrogen bonding between hydroxy groups at the interlayer surface.[29,30] In contrast, the absorbance at 3650 cm^{-1} was disappeared after the modification with initiator **1** because OH groups on the magadiite interlayer surface reacted with silyl chloride to form covalent bonds.

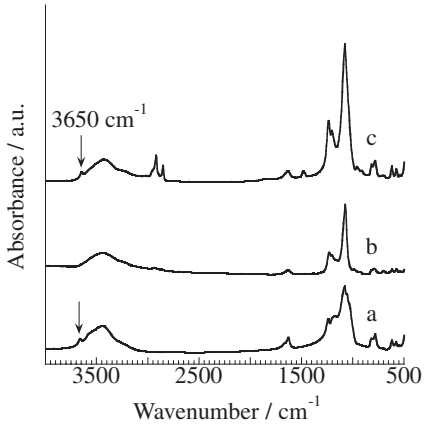

Figure 3. Infrared spectra of a series of magadiite derivatives. (a) Na-magadiite, (b) **1**-magadiite, and (c) DTMA-magadiite.

Table II. SEC analysis of PS chains and magadiite content in PS/magadiite nanocomposites as a function of time[a]

Sample	temp, K	time, h	conversion, %[a]	$M_n \times 10^{-3}$		PDI[c]	Magadiite content, wt %[d]
				calcd[b]	obsd[c]		
1	398	1	6	2.8	59	1.39	26
2	398	3	24	11	114	1.60	10
3	398	6	34	15	214	1.73	5

[a]Conversion, % = (weight of PS/magadiite nanocomposites − weight of **1**-magadiite)/(initial weight of styrene monomer) × 100. [b]M_n (calcd) = $([M]_0/[I]_0) \times M_w$ of styrene × conversion)/100. $[M]_0 = 21.6$ mmol, $[I]_0 = 0.05$ mmol. [c]Measured by SEC using PS standards in THF at 313 K. [d]Estimated by TGA.

Characterization of PS Chains on PS/Magadiite Nanocomposites as a Function of Time

The amount of initiator immobilized on the magadiite interlayer surface was determined from elemental analysis, as shown in Table I. The molar ratio of styrene monomer and surface initiator was set to be 21.6 to 0.05 mmol, respectively. The polymerization results are shown in Table II. The refined PS nanocomposites were treated with 3% hydrofluoric acid aqueous solution at room temperature for 24 h, leading to bond cleavage between anchored PS chains and the magadiite interlayer surface to isolate the anchored PS chains sorely. The M_n of the cleaved PS chains was determined by SEC. The M_n increased with the polymerization time from 59000 to 214000. Magadiite content in nanocomposites determined by TGA analysis decreased from 26 to 5 wt % with increases in the M_n of grafted-PS. Thus, the magadiite content in PS matrices can be controlled by the degree of polymerization. As shown in Table II, the grafted PS had considerably larger M_n's than the theoretical values calculated by the feed molar ratio of monomer and the amount of surface initiator, indicating the low initiator efficiency. Only 8% of surface initiator actually started polymerization of styrene probably due to the heterogeneous polymerization condition and steric hindrance around the initiators restricted quantitative initiation.

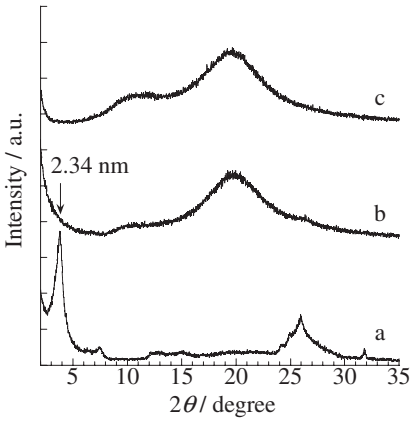

Figure 4. XRD patterns of PS/magadiite nanocomposites. (a) **1**-magadiite; $d_{001} = 2.34$ nm, (b) PS/magadiite nanocomposites containing 5 wt % of magadiite prepared by means of surface-initiated polymerization for 6 h, and (c) pure PS.

Figure 4 shows XRD patterns of **1**-magadiite and PS/magadiite nanocomposites. No diffraction peak derived from the basal spacing of magadiite layers was observed in the XRD pattern of PS/magadiite nanocomposites, indicating delamination of magadiite in the PS matrices.

The Observation of Magadiite Dispersion States in PS Matrices

Figure 5 shows representative transmission optical microscopy images of various PS/magadiite composites containing 5 wt % of magadiite in the PS matrices and pure PS. The employed pure PS, which is amorphous polymers without magadiite, exhibits transparency, as shown in Figure 5(a). A series of PS/magadiite composites prepared by a coagulation method are opaque, as shown in Figure 5(b) to 5(d). The results are caused by poor dispersion of magadiite in PS matrices. Diffraction peaks derived from basal spacings of magadiite layers were observed by XRD. In contrast, PS/magadiite nanocomposites prepared by surface-initiated polymerization did not have agglomerated particles as shown in Figure 5(e). The result suggests delaminated structures of magadiite in PS matrices on at least micron scales. Thus, some properties of the delaminated PS/magadiite nanocomposites can be expected to be superior to those of the PS/magadiite composites with agglomerated structures because of an improvement in the dispersion state of magadiite in PS matrices. The PS/magadiite nanocomposites exhibited better transparency than that of any other PS/magadiite composites prepared by the coagulation method.

TEM images of a series of PS composites are shown in Figure 6. The dark and light parts in the figure correspond to magadiite layers and PS, respectively. For a series of PS/magadiite composites prepared by a coagulation method, laminated structures of magadiite were observed, as seen in Figure 6(b) to 6(d). In contrast, as seen in Figure 6(e), delaminated structures of magadiite were observed for PS/magadiite nanocomposites prepared by surface-initiated polymerization. The intervals between exfoliated magadiite layers

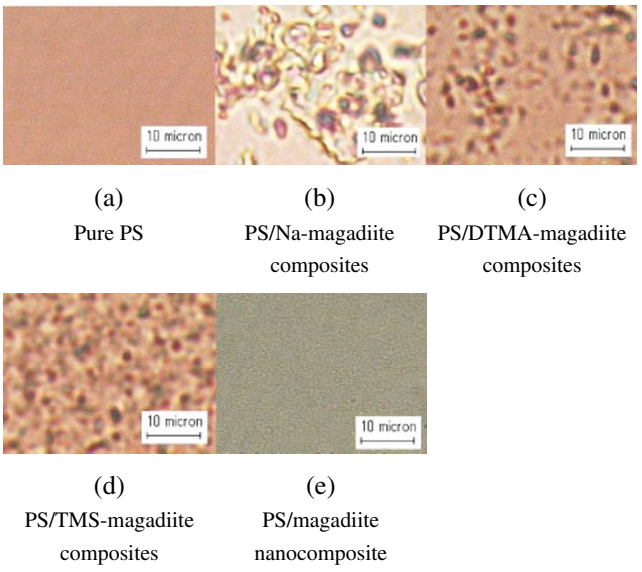

(a) Pure PS (b) PS/Na-magadiite composites (c) PS/DTMA-magadiite composites

(d) PS/TMS-magadiite composites (e) PS/magadiite nanocomposite

Figure 5. Optical microscopy images of a series of PS composites. (a) Pure PS, (b) PS/Na-magadiite composites containing 5 wt % of magadiite prepared by a coagulation method, (c) PS/DTMA-magadiite composites containing 5 wt % of magadiite prepared by a coagulation method, (d) PS/TMS-magadiite composites containing 5 wt % of magadiite prepared by a coagulation method, and (e) PS/magadiite nanocomposites containing 5 wt % of magadiite prepared by surface-initiated polymerization. Scale bars are 10 μm. All samples were placed on a hot stage at a high temperature of 573 K in a nitrogen stream of 50 mL/min and observed at melt state.

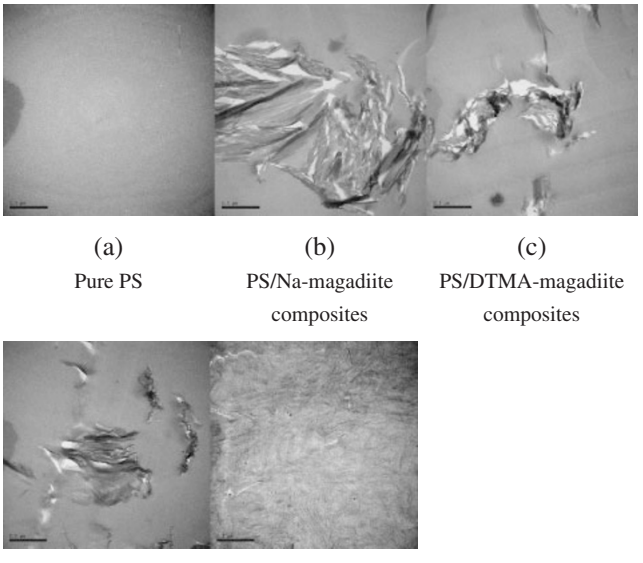

(a) Pure PS (b) PS/Na-magadiite composites (c) PS/DTMA-magadiite composites

(d) PS/TMS-magadiite composites (e) PS/magadiite nanocomposites

Figure 6. TEM images of a series of PS composites. (a) Pure PS, (b) PS/Na-magadiite composites containing 5 wt % of magadiite, (c) PS/DTMA-magadiite composites containing 5 wt % of magadiite, (d) PS/TMS-magadiite composites containing 5 wt % of magadiite, and (e) PS/magadiite nanocomposites containing 5 wt % of magadiite. Thin films measure 50 nm thick. Scale bars are 500 nm.

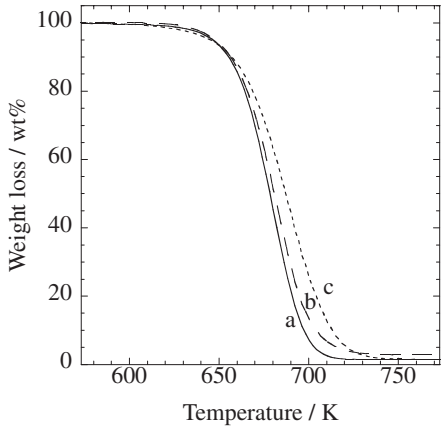

Figure 7. TG curves of a series of PS composites. (a) Pure PS; solid line, (b) PS/DTMA-magadiite composites containing 5 wt % of magadiite; broken line, and (c) PS/magadiite nanocomposites containing 5 wt % of magadiite; dotted line. Thermal degradation behaviors of the samples were measured by TGA in a nitrogen stream of 200 mL/min at a heating rate of 10 K/min from 303 to 1173 K. The plots of PS/Na-magadiite and PS/TMS-magadiite composites were omitted because they showed similar thermal degradation curves to that of PS/DTMA-magadiite ones in the figure.

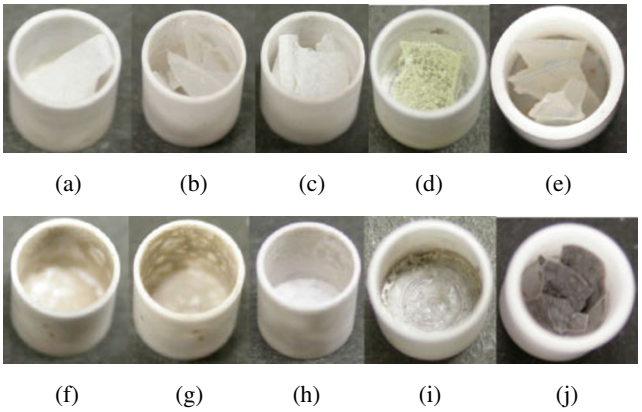

Figure 8. Photo images of the final residues of a series of PS composites before and after TGA. (a) PS/Na-magadiite composites containing 5 wt % of magadiite before TGA, (b) PS/DTMA-magadiite composites containing 5 wt % of magadiite before TGA, (c) PS/TMS-magadiite composites containing 5 wt % of magadiite before TGA, (d) PS/magadiite nanocomposites containing 1 wt % of magadiite before TGA, (e) PS/magadiite nanocomposites containing 5 wt % of magadiite before TGA, (f) PS/Na-magadiite composites containing 5 wt % of magadiite after TGA, (g) PS/DTMA-magadiite composites containing 5 wt % of magadiite after TGA, (h) PS/TMS-magadiite composites containing 5 wt % of magadiite after TGA, (i) PS/magadiite nanocomposites containing 1 wt % of magadiite after TGA, and (j) PS/magadiite nanocomposites containing 5 wt % of magadiite after TGA. The final residues of a series of PS composites were obtained from TGA analysis in a nitrogen stream of 200 mL/min at a heating rate of 10 K/min from 303 to 1173 K.

were measured to be around 30 to 50 nm. This result is probably due to the growth of PS, which was inserted by nitroxide-mediated radical polymerization from the **1**-magadiite interlayer surface.

We can therefore conclude that a very effective approach for the exfoliation of magadiite in PS matrices is to immobilize sufficient amounts of nitroxide-mediated radical initiators onto the magadiite interlayer surface where PS chains with relative narrow polydispersities are grown by means of surface-initiated polymerization of styrene.

Relationship between Dispersion States of Magadiite in PS Matrices and Their Thermal Degradation Behaviors

Thermal degradation behaviors of a series of PS composites were analyzed by TGA. TG curves of the exfoliated PS/magadiite nanocomposites shifted toward a higher temperature region than those of any other employed PS composites with agglomerated structures. Figure 7 shows that the exfoliated PS/magadiite nanocomposites possess higher thermal stability.

Since Blumstein and his coworkers first reported the improvement in thermal stability of a polymer clay nanocomposite consisting of poly(methyl methacrylate) and MMT in 1965,[31] various polymer nanocomposites with good thermal stabilities have been reported thus far.[32,33] In addition, we have demonstrated that an enhancement in thermal stability at PS/magadiite nanocomposites be caused by an improvement in the dispersion of magadiite in the PS matrices at a nano scale. In other words, the increase in interface areas between the PS matrices and the individual surfaces of delaminated magadiite platelets is very effective at suppressing the thermal degradation of the PS matrices.

Figure 8 shows photo images of final residues for a series of PS composites before and after TGA. Pure PS was completely decomposed during thermal degradation at high temperatures

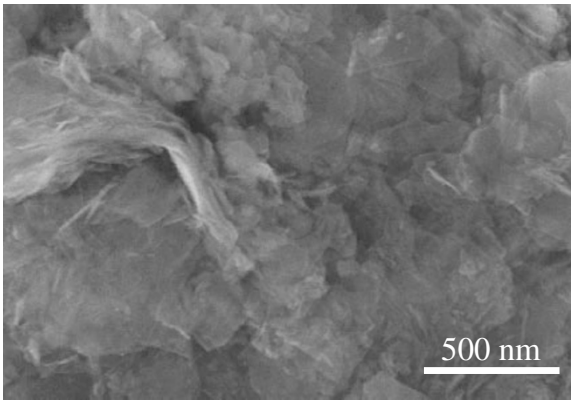

Figure 9. Representative STEM image of the final residues of exfoliated PS/magadiite nanocomposites containing 5 wt % of magadiite after TGA. Scale bar is 500 nm.

to give no residues. In contrast, for exfoliated PS/magadiite nanocomposites containing 5 wt % of magadiite, the final residues remained as substantially rigid solids, maintaining their shape, as shown in Figure 8(e) and 8(j). Figure 9 shows the STEM image of the final residue of exfoliated PS/magadiite nanocomposites containing 5 wt % of magadiite after TGA. The residues shown in Figure 9 represent only a large gathering of individual exfoliated magadiite layers because the PS matrix was completely decomposed during thermal degradation, indicating that the residues are made up of a large amount of exfoliated magadiite layers to form continuous layers. These results suggest that the seamless solids formed by exfoliated magadiite layers keep in the range of nano to macro

scales as shown in Figure 9 and Figure 8(j). Figure 8(i) shows final residues of exfoliated PS/magadiite nanocomposites containing 1 wt % of magadiite after TGA. In contrast to Figure 8(j), a small amount of silicate powder was observed for the low concentrations of exfoliated magadiite in PS matrices. The seamless solid formation of the final residue depended on the concentration of delaminated magadiite in PS matrices, as shown in Figure 8(i) and 8(j). In contrast, the final residues of all aggregated PS/magadiite composites containing 5 wt % of magadiite turned to an ash-shaped powder, as shown in Figure 8(f) to (h). The difference in the shapes of the final residues was clearly affected by the magadiite dispersion states such as aggregated or delaminated structures and the concentrations in PS matrices. The seamless solid formation takes place under the conditions of exfoliated dispersion and high concentrations of magadiite in PS matrices.

Magadiite is inactive for the flame of combustion. Therefore, for the exfoliated magadiite to form continuous layers to cover the PS matrices, the layers will serve as a protective barrier for underlying PS matrices against flame and will obstruct the progress of fuel gases toward the flame during combustion. Consequently, the exfoliated PS/magadiite nanocomposites will demonstrate higher flame-retardant performance.

CONCLUSIONS

Exfoliated PS/magadiite nanocomposites were successfully prepared by means of *in situ* nitroxide-mediated radical polymerization from the initiator-immobilized magadiite interlayer surface. They have better transparency than that of any other PS/magadiite composites prepared by the coagulation method. The suppression effect on thermal degradation was enhanced by the delaminated dispersion of magadiite in PS matrices. In addition, an interesting difference in the shapes of final residues occurred among a series of PS/magadiite composites. For exfoliated PS/magadiite nanocomposites, the final residues remained as substantially rigid solids, maintaining their shape. The solid formation depended on the concentrations of magadiite in PS matrices. The seamless solid residue is synthesized under conditions of the exfoliated dispersion and high concentrations of magadiite in PS matrices. Magadiite is inactive for the flame of combustion. Therefore, as the exfoliated magadiite forms continuous layers to cover the PS matrices, the layers will act as a protective barrier for underlying PS matrices against flame and obstruct the progress of fuel gases toward the flame during combustion. Consequently, the exfoliated PS/magadiite nanocomposites will demonstrate higher flame-retardant performance.

Acknowledgment. The authors thank to Mr. Yuyu Ohnuma, Mr. Akio Hashizume, Dr. Kenichirou Hiwatari, and Dr. Ryoji Kimura in ADEKA Corporation for supporting and providing TMS-magadiite.

Received: February 20, 2009
Accepted: April 1, 2009
Published: May 27, 2009

REFERENCES

1. K. Takeda, F. Amemiya, M. Kinoshita, and S. Takayama, *J. Appl. Polym. Sci.*, **64**, 1175 (1997).
2. Y. Kojima, A. Usuki, M. Kawasumi, A. Okada, T. Kurauchi, and O. Kamigaito, *J. Polym. Sci., Part A: Polym. Chem.*, **31**, 983 (1993).
3. M. Alexandre and P. Dubois, *Mater. Sci. Eng., R*, **28**, 1 (2000).
4. N. Hasegawa, H. Okamoto, M. Kawasumi, and A. Usuki, *J. Appl. Polym. Sci.*, **74**, 3359 (1999).
5. J. W. Gilman, *Appl. Clay Sci.*, **15**, 31 (1999).
6. B. Morgan, R. H. Harris Jr, T. Kashiwagi, L. J. Chyall, and J. W. Gilman, *Fire Mater.*, **26**, 247 (2002).
7. Laachachi, E. Leroy, M. Cochez, M. Ferriol, and J. M. L. Cuesta, *Polym. Degard. Stab.*, **89**, 344 (2005).
8. T. Kashiwagi, A. B. Morgan, J. M. Antonucci, M. R. Vanlandingham, R. H. Harris Jr, W. H. Awad, and J. R. Shields, *J. Appl. Polym. Sci.*, **89**, 2072 (2003).
9. T. Kashiwagi, E. Grulke, J. Hilding, K. M. Groth, R. Harris, K. Butler, J. Shields, S. Kharchenko, and J. Douglas, *Polymer*, **45**, 4227 (2004).
10. T. Kashiwagi, F. Du, J. F. Douglas, K. I. Winey, R. H. Harris Jr, and J. R. Shields, *Nat. Mater.*, **4**, 928 (2005).
11. T. Kashiwagi, F. Du, K. I. Winey, K. M. Groth, J. R. Shields, S. P. Bellayer, H. Kim, and J. F. Douglas, *Polymer*, **46**, 471 (2005).
12. E. Devaux, S. Bourbigot, and A. E. Achari, *J. Appl. Polym. Sci.*, **86**, 2416 (2002).
13. P. Jash and C. A. Wilkie, *Polym. Degard. Stab.*, **88**, 401 (2005).
14. M. W. Weimer, H. Chen, E. P. Giannelis, and D. Y. Sogah, *J. Am. Chem. Soc.*, **121**, 1615 (1999).
15. C. Konn, F. Morel, E. Beyou, P. Chaumont, and E. Bourgeat-Lemi, *Macromolecules*, **40**, 7464 (2007).
16. M. Moniruzzaman and K. I. Winey, *Macromolecules*, **39**, 5194 (2006).
17. S. Okutomo, K. Kuroda, and M. Ogawa, *Appl. Clay Sci.*, **15**, 253 (1999).
18. K. Kosuge and A. Tsunashima, *Langmuir*, **12**, 1124 (1996).
19. D. Wang, D. D. Jiang, J. Pabst, Z. Han, J. Wang, and C. A. Wilkie, *Polym. Eng. Sci.*, **44**, 1122 (2004).
20. K. Isoda, K. Kuroda, and M. Ogawa, *Chem. Mater.*, **12**, 1702 (2000).
21. Y. Ide and M. Ogawa, *Nendo Kagaku*, **46**, 200 (2007).
22. C. J. Hawker, G. G. Barclay, A. Orellana, J. Dao, and W. Devonport, *Macromolecules*, **29**, 5245 (1996).
23. Y. Wang, J. Cai, H. Rauscher, R. J. Behm, and W. A. Goedel, *Chem. Eur. J.*, **11**, 3968 (2005).
24. K. Kosuge, A. Yamazaki, A. Tsunashima, and R. Otsuka, *J. Ceram. Soc. Jpn.*, **100**, 326 (1992).
25. C. Eypert-Blaison, E. Sauzéat, M. Pelletier, L. J. Michot, F. Villiéras, and B. Humbert, *Chem. Mater.*, **13**, 1480 (2001).
26. R. A. Vaia, R. K. Teukolsky, and E. P. Giannelis, *Chem. Mater.*, **6**, 1017 (1994).
27. E. R. Hitzky, J. M. Rojo, and G. Lagaly, *Colloid Polym. Sci.*, **263**, 1025 (1985).
28. S. Peng, Q. Gao, Q. Wang, and J. Shi, *Chem. Mater.*, **16**, 2675 (2004).
29. H. Muraishi, *Nendo Kagaku*, **44**, 62 (2004).
30. S. Okutomo, K. Kuroda, and M. Ogawa, *Appl. Clay Sci.*, **15**, 253 (1999).
31. A. Blumstein, *J. Polym. Sci., Part A: Polym. Chem.*, **3**, 2653 (1965).
32. W. Dong, X. Zhang, Y. Liu, Q. Wang, H. Gui, J. Gao, Z. Song, J. Lai, F. Huang, and J. Qiao, *Polymer*, **47**, 6874 (2006).
33. G. Beyer, *Fire Mater.*, **25**, 193 (2001).